Article:
Li, H., Chen, X. and Zhu, Z.Q. (2026) Online monitoring of internal ground-wall insulation in permanent magnet synchronous machines. IEEE Transactions on Transportation Electrification. p. 1. ISSN: 2577-4212

https://doi.org/10.1109/tte.2026.3665866

Online Monitoring of Internal Ground-wall Insulation in Permanent Magnet Synchronous Machines

Huanyu Li, Student Member, IEEE, Xiao Chen, Senior Member, IEEE, Zi Qiang Zhu, Fellow, IEEE

***Abstract*—For inverter-driven permanent magnet synchronous machines (PMSMs), the transient overvoltage phenomenon at the machine line-end has attracted widespread attention because of its potential to degrade the winding insulation, thereby causing premature failure. For this issue, various line-end ground-wall (GW) insulation monitoring methods have been proposed. However, recent research indicates that, in addition to the line-end, significant overvoltage also occurs inside the windings. In some cases, the internal overvoltage even exceeds the line-end overvoltage. Therefore, it is necessary to develop an online internal GW insulation monitoring method. This paper first establishes a high-frequency winding model, which can be used to study the effects of GW insulation aging at different positions. This study demonstrates that when the internal GW insulation degradation occurs, the common-mode (CM) impedance antiresonance frequency changes. It also shows that the natural frequency of the CM circuit is equal to the CM impedance antiresonance frequency. Therefore, this paper proposes an insulation monitoring method based on the system's natural frequency. This method can quantitatively detect the internal GW insulation aging. To accurately extract the natural frequency of the system, a transfer function-based frequency extraction method is proposed. The performance of the proposed method is not affected by switching frequency and modulation index, demonstrating its strong robustness. Both distributed and concentrated winding PMSMs are employed for experimental validation.**

***Index Terms*— CM impedance, insulation aging, natural frequency, neutral point overvoltage, transfer function-based frequency extraction.**

I. INTRODUCTION

In recent decades, increasingly more permanent magnet synchronous machines (PMSMs) have been applied in various industries, such as hybrid and electric vehicles, wind turbines, and aerospace, etc. [1-3]. Unlike mains-fed machines, due to the steep fronted voltage generated by the voltage source inverter (VSI), the voltages in VSI-fed PMSMs contain not only the fundamental component but also many high frequency (HF) components. HF components can cause transient overvoltage [4], which accelerates the aging of the winding ground-wall (GW) insulation. Investigation shows that the stator winding insulation is a relatively fragile component, accounting for approximately 40% of machine failures and once it experiences early failure, it degrades rapidly [5][6]. Therefore, it is necessary to monitor the GW insulation in real time to provide early warnings before a fault occurs, which is critical for high-reliability applications.

Insulation aging is physically manifested by changes in dielectric properties and geometry, primarily affecting the equivalent capacitance. Under dominant thermal stress, chemical decomposition and delamination introduce air voids, reducing the effective dielectric constant and decreasing capacitance [7]. Conversely, moisture ingress increases the effective dielectric constant, leading to higher capacitance [8]. Furthermore, as aging reduces the partial discharge inception voltage (PDIV), the internal partial discharges at high operating voltages can cause a 'tip-up' in capacitance, as the ionization of gas within voids increases the effective permittivity [9]. Therefore, insulation capacitance value can be regarded as a key indicator of GW insulation degradation. In the early days, the GW insulation capacitance was calculated by measuring the common-mode (CM) leakage current at multiples of the line frequency [10]. However, due to the large impedance of the GW insulation capacitor at low frequencies, the CM leakage current is very small, thus an expensive high-sensitivity current sensor is needed [10]. To solve this problem, PWM frequency and its harmonics are used to calculate the GW insulation capacitance [11], [12]. In addition to directly monitoring insulation capacitance, other features can also be used for insulation monitoring, such as partial discharge (PD) [13], impedance spectrum [14], [15] and switching transient currents [16]-[19]. Online PD tests are mainly applicable to high-voltage machines, and in inverter-fed machines, PD signals are easily affected by HF noise. In [15], the phase-to-ground impedance spectrum is measured by HF injection method to monitor the GW insulation. In inverter-fed machines, HF switching transient currents exist in the windings due to rapid switching actions, which can be also used for insulation monitoring [16]-[19].

The above methods mainly focus on monitoring the overall GW insulation. However, for inverter-driven PMSMs, the line-end coil is generally considered to be more prone to aging due to the overvoltage phenomenon at the line-end terminal. Fig. 1 shows the widely used HF common-mode electrical machine model, which is valid in medium frequency and HF regions (e.g., 50kHz–1MHz), established using lumped parameters [20]. C_{g1} represents the lumped parasitic capacitance of the "entry section" of the stator winding. In [21], the line-end coil is defined as the first coil of phase winding that enters the machine. C_{g2} is the internal GW capacitance, C_t represents the interturn capacitance, and r and

Huanyu Li, Xiao Chen and Zi Qiang. Zhu are with the School of Electrical and Electronic Engineering, The University of Sheffield, Sheffield S1 3JD, U.K. (e-mail: hli209@sheffield.ac.uk; xiao.chen@sheffield.ac.uk; z.q.zhu@sheffield.ac.uk). (Corresponding author: Xiao Chen).

L are the resistance and inductance of stator windings, respectively. R represents HF losses, including the iron loss and the copper loss, influenced by the skin and proximity effects. At present, some scholars have conducted some research to monitor the line-end coil capacitance C_{g1} [21], [22]. In [21], the line-end GW insulation is monitored by switching oscillation mode decomposition. The parity-time symmetry is used to monitor the line-end GW insulation in [22].

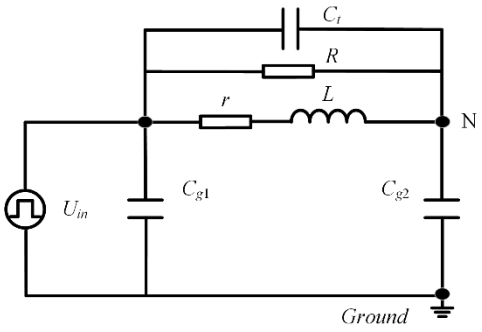

Fig. 1. CM electrical machine equivalent model [20].

In fact, recent studies indicate that, due to antiresonance phenomena, significant overvoltage also occurs inside the windings [23]. Therefore, it is equally necessary to monitor the internal GW insulation of the windings. In [24], the HF oscillation of the neutral point voltage is utilized to monitor the internal GW insulation, with the Fast Fourier Transform (FFT) employed to extract the oscillation frequency. However, this method is affected by voltage waveform aliasing.

To more accurately monitor the internal GW insulation, this paper first establishes a multiconductor transmission line (MCTL)-based model to capture the HF behavior of the electrical machine windings. Based on this model, the effect of GW insulation aging at different locations on the antiresonance frequency of the CM impedance spectrum is studied. The results show that aging of internal GW insulation can alter the antiresonance frequency of the CM impedance spectrum. Online monitoring of the CM impedance spectrum has been explored in [14]. However, reliable calculation is restricted to specific frequencies with sufficiently large amplitudes, which means that the impedance spectrum is discrete. While this discrete information suffices for monitoring general impedance trends, it lacks the frequency resolution required to accurately pinpoint the antiresonance frequency, a critical indicator for internal GW insulation status. To address this limitation, this paper proposes a new monitoring indicator, which is the natural frequency of the second-order system consisting of the machine's CM circuit. This study shows that this frequency is equal to the CM impedance antiresonance frequency. Therefore, it can be used as a substitute for the CM impedance antiresonance frequency in insulation monitoring. To accurately extract the natural frequency of the system, the nonlinear least squares method is used to identify the system transfer function, and then the natural frequency is calculated. The proposed insulation monitoring method can quantitatively detect the internal GW insulation aging and is not affected by the line-end GW insulation degradation. In addition, the proposed natural frequency extraction method has strong robustness. Both distributed and concentrated winding PMSMs are employed for experimental validation.

The rest of this article is organized as follows. Section II presents the multiconductor transmission lines (MCTL) model of the stator winding. An internal GW insulation monitoring method is proposed in Section III. In Section IV and Section V, simulation results and experimental results are respectively presented to support the proposed insulation monitoring method. Finally, Section VI concludes this article.

II. Multiconductor Transmission Line Model of Machine Winding

A. High Frequency Model of Machine Winding

To study the effect of insulation aging at different positions, it is necessary to establish a HF model of the winding. The winding HF model can be classified into three categories: the behavior-based model [25], the finite element (FE)-based model [26], and the MCTL-based model [23], [27].

The behavior-based model uses measured data to establish a lumped parameter model of the winding, which requires the physical availability of machine windings. The FE-based model utilizes finite element software to conduct a field-circuit coupled analysis of the machine. Due to the model's complexity and the necessity for a small-time step, solving it often requires a significant amount of time. For instance, in [26], a single simulation (1μs) with a time step of 2ns takes approximately four weeks to complete on a computer equipped with 4 cores and 64 GB of memory.

According to MCTL theory [28], stator windings can be represented using lumped parameter equivalent circuits, if the winding length represented by the basic unit is much smaller than the wavelength corresponding to the maximum frequency to be considered. The detailed modeling process for an MCTL-based approach is shown in [23], [27]. Specifically, the method outlined in [23] is suitable for cases where the number of conductors per slot is relatively low. When many conductors are present in a single slot, homogenization techniques can be employed to simplify calculations [27]. This paper adopts the MCTL-based model as the foundation for the research.

B. Multiconductor Transmission Line-based Model

As the modeling process is not the focus of this paper, only a brief description will be provided. The detailed modeling process can be found in [23]. The modeling process consists of four key steps:

Step 1: Establishment of an FE model

This paper first establishes an FE model in ANSYS Maxwell for extracting winding impedance parameters. The prototype analyzed in this paper is a 60 kW PMSM from the 2010 Toyota Prius. Detailed machine parameters used for FE modeling are provided in the appendix [23]. To consider the skin and proximity effects of windings at high frequencies,

each conductor is individually modelled, as illustrated in Fig. 2.

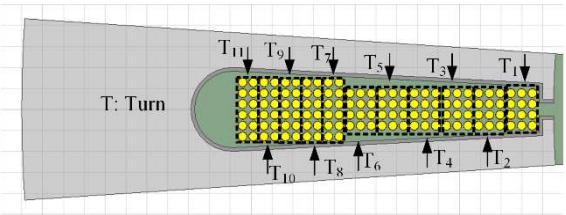

Fig. 2. Cross-section of a single slot.

Step 2: Extraction of turn impedance parameters at various frequencies

At high frequencies, the winding behavior cannot be accurately represented using simple RL circuits due to the influence of parasitic capacitance. Therefore, each cell in the MCTL-based model, representing a single turn, includes the following key parameters:

1) Turn self-inductance and resistance.
2) Turn mutual inductance and resistance.
3) Turn-to-ground capacitance and turn-to-turn capacitance: Turn-to-ground capacitance is the capacitance that characterizes the GW insulation.
4) Overhang inductance: Represents the inductance of a turn in the end-winding region

Specifically, the inductance and resistance are obtained through eddy current field solvers at 10 Hz, 100 Hz, 1 kHz, 10 kHz, 100 kHz, 1 MHz and 10 MHz, while turn-to-ground capacitance and turn-to-turn capacitance are obtained through electrostatic field solvers. The overhang inductance is obtained based on formula 8 in [23].

Step 3: Parameter fitting

The impedance values vary with frequency due to skin and proximity effects. To enable transient voltage analysis in the time domain, it is necessary to express these impedance values as functions of frequency. For this purpose, a sixth-order RL ladder circuit is employed to approximate the self-impedance and mutual impedance of each turn over a broad frequency range. The parameters of the ladder circuit are obtained through a fitting process, as discussed in [23]. Fig. 3 presents a comparison between the ladder circuit model and FEA results for the self-impedance variation of turn 1 at different frequencies. The results demonstrate that the sixth-order RL ladder circuit effectively captures the impedance variation. It is worth noting that since the maximum frequency used for fitting the lumped parameter circuit is 10 MHz, the leakage inductance effects induced by the high-frequency components of the PWM step edges (beyond this frequency) cannot be accurately captured. However, as the frequencies investigated in this study do not exceed 10 MHz, such modeling errors are considered acceptable.

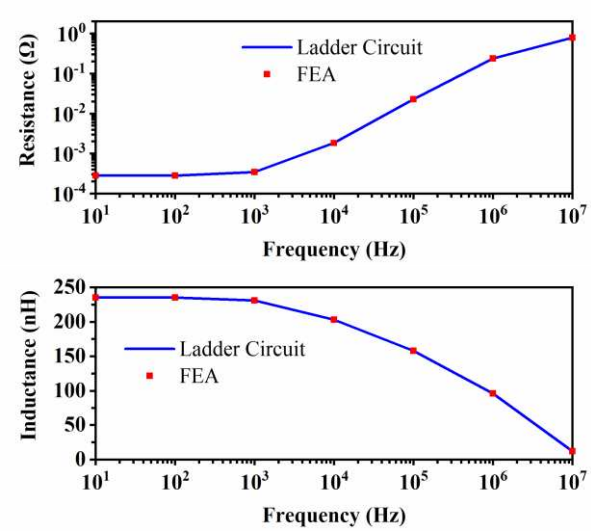

Fig. 3. Comparison between ladder circuit and FEA about variation of the self-impedance with frequency for turn 1.

Step 4: Establishment of a MCTL-based model

With all necessary parameters extracted, a complete MCTL-based model is implemented in MATLAB/Simulink. Fig. 4 shows the MCTL-based model structure of one phase. Among them, C_{tt} is the turn-to-turn capacitance, and C_{tg} is the turn-to-ground capacitance. According to the winding connection method, the three-phase windings can be connected in a star shape. Fig. 5 illustrates the comparison between experimentally measured and simulated machine CM impedances. Due to the simplification of the model regarding random winding distribution and high-frequency iron loss, and assuming that all coil parameters are the same, the difference in impedance amplitude is observed in Fig. 5, which mainly occurs in the frequency band significantly higher than the antiresonance frequency. However, the simulated antiresonance frequency (291 kHz) is highly consistent with the experimental data (294 kHz). Due to the dependence of the proposed monitoring indicators on antiresonance frequency shift, this model provides an effective and robust foundation for the proposed method.

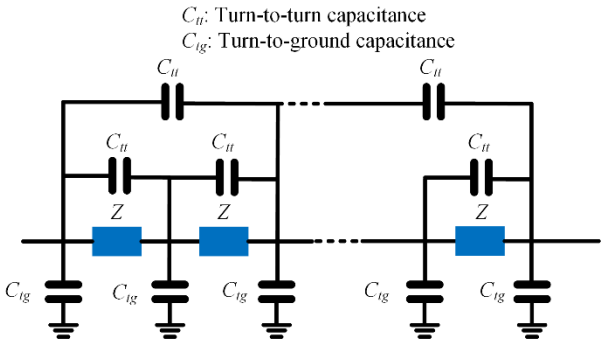

Fig. 4. MCTL-based model structure of one phase.

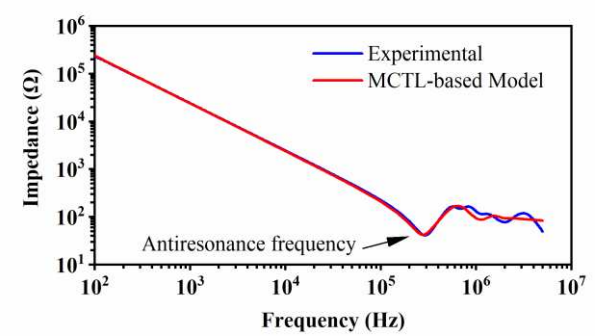

Fig. 5. Comparison of measured and simulated CM impedances.

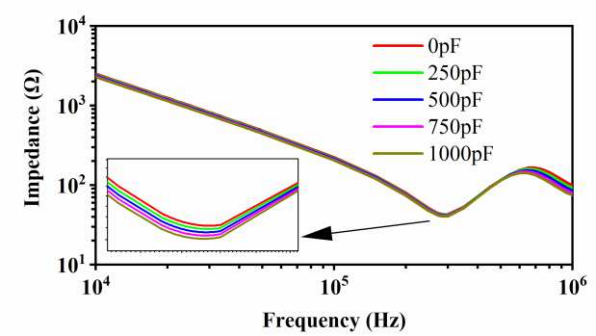

Fig. 7. CM impedance spectra under line-end GW insulation aging.

III. Internal GW Insulation Aging Monitoring Method

A. Effect of GW Insulation Aging on CM Impedance

Empirical studies from accelerated aging tests demonstrate that a capacitance variation range of less than 50% is considered to physically represent the transition from initial degradation to potential faults [7], [22]. In this study, the internal GW insulation capacitance of the test machine was identified as approximately 2200 pF using the parameter identification method described in [29]. Accordingly, internal GW insulation degradation was simulated by connecting external capacitors of 250 pF, 500 pF, 750 pF, and 1000 pF in parallel between the neutral point and ground. These values correspond to variations well within the 50% range, ensuring the simulation setup adheres to the realistic degradation laws observed in the literature. Although parallel capacitor connection only simulates capacitance increase scenarios, it is sufficient to verify the sensitivity and effectiveness of the proposed monitoring method. The effect of internal GW insulation aging on the CM impedance spectrum is illustrated in Fig. 6. It is observed that the internal GW insulation aging alters the antiresonance frequency of the CM impedance. For comparison, a capacitor is inserted at the line-end to simulate the line-end GW insulation aging. The simulation results, shown in Fig. 7, indicate that the degradation of the line-end GW insulation does not affect the CM impedance antiresonance frequency.

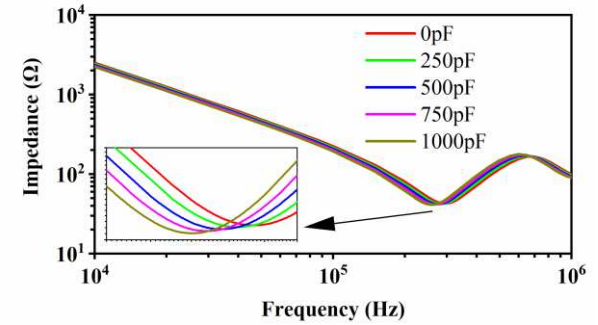

Fig. 6. CM impedance spectra under internal GW insulation aging.

The above phenomenon can be explained as follows. Since the resistance r is much smaller than the inductive reactance (ωL) in the high-frequency region, r is ignored in Fig. 1 [20]. And the CM impedance Z_{cm} can be derived as follows.

$$Z_{cm} = \frac{L(C_{g2}+C_t)s^2 + \frac{L}{R}s + 1}{(C_{g1}+C_{g2})s\left[L\left(C_t + \frac{C_{g1}C_{g2}}{C_{g1}+C_{g2}}\right)s^2 + \frac{L}{R}s + 1\right]} \quad (1)$$

According to (1), the antiresonance frequency of CM impedance spectrum can be derived as (2) [20].

$$f_r = \frac{1}{2\pi\sqrt{L(C_t + C_{g2})}} \quad (2)$$

From (2), the antiresonance frequency is not affected by the line-end GW capacitance C_{g1}, while a change in internal GW capacitance C_{g2} will alter the antiresonance frequency. Therefore, the antiresonance frequency of CM impedance spectrum can be used to monitor the internal GW insulation aging. However, it is very difficult to obtain the CM impedance antiresonance frequency online. Therefore, it is necessary to find an easily accessible indicator that can replace the antiresonance frequency.

B. A New Insulation Aging Monitoring Indicator

Fig. 8 shows the ideal and actual neutral point voltages with the MCTL-based model. In this simulation, the inverter switching state changes from 000 to 111. The DC bus voltage U_{DC} is 100V. Due to the influence of parasitic parameters, the neutral point voltage is not an ideal step wave, and there is an obvious voltage oscillation. In existing literature [23] [24], the authors believe that the oscillation frequency of neutral point voltage is equal to the antiresonance frequency of CM impedance spectrum. And the oscillation frequency of neutral point voltage is used for insulation monitoring in [24]. However, this paper finds that the oscillation frequency of the neutral point voltage is not equal to the antiresonance frequency of the CM impedance spectrum, while the natural frequency of the CM circuit (the new monitoring indicator proposed in this paper) is exactly equal to the antiresonance frequency of the CM impedance spectrum. And this study also finds that when the internal GW insulation degradation occurs, the relative change in the oscillation frequency of the neutral

point voltage is less than the relative change in the natural frequency. A detailed derivation will be given later in this section. Therefore, this paper proposes a new indicator (natural frequency) to replace the antiresonance frequency of the CM impedance spectrum for insulation monitoring.

For Fig. 1, taking the neutral point voltage (the voltage across C_{g2}) as the output while taking the CM voltage (average value of the three-phase voltages between the terminals and the midpoint of the DC bus) as the input, the transfer function can be derived. The expression of the transfer function is shown in (3), which is a second-order transfer function with two poles and two zeros. For a second-order transfer function, its denominator can be expressed as a general expression as shown in (4), where ω_n is the natural angular frequency of the second-order system, ξ is the damping ratio of the second-order system, which can be expressed by (5) and (6) respectively. And the natural frequency f_n of the second-order system can be derived from (5). For a second-order underdamped system ($0 < \xi < 1$), the damped natural frequency f_d is the actual response frequency under the step input, which can be represented by (8). The neutral point voltage oscillation frequency can be approximately equal to the damped natural frequency. Comparing (2), (7), and (8), it can be observed that the antiresonance frequency of the CM impedance is equal to the natural frequency f_n rather than the damped natural frequency f_d (neutral point voltage oscillation frequency).

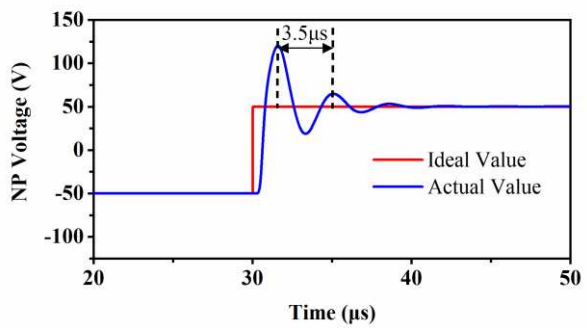

Fig. 8. Ideal and actual neutral point (NP) voltage with the MCTL-based model.

$$G(s) = \frac{RLC_t s^2 + Ls + R}{RL(C_{g2} + C_t)s^2 + Ls + R} \tag{3}$$

$$G_d(s) = s^2 + 2\xi\omega_n s + \omega_n^2 \tag{4}$$

$$\omega_n = \frac{1}{\sqrt{L(C_{g2} + C_t)}} \tag{5}$$

$$\xi = \frac{1}{2R}\sqrt{\frac{L}{C_{g2} + C_t}} \tag{6}$$

$$f_n = \frac{\omega_n}{2\pi} = \frac{1}{2\pi\sqrt{L(C_{g2} + C_t)}} \tag{7}$$

$$f_d = f_n\sqrt{1 - \xi^2} = \frac{1}{2\pi}\sqrt{\frac{4R^2(C_{g2} + C_t) - L}{4R^2L(C_{g2} + C_t)^2}} \tag{8}$$

According to (7), it is obvious that the natural frequency is inversely proportional to the square root of GW capacitance C_{g2}. For the damped natural frequency, it is necessary to take its derivative to determine its relationship with the insulation capacitance C_{g2}. For the sake of simplicity, only the expression in the square root of (8) needs to be differentiated, and the result is shown in (9).

$$\frac{\partial f_{d\_sr}}{\partial C_{g2}} = \frac{\left[8R^2L(C_{g2} + C_t)\right] \times \left[L - 2R^2(C_{g2} + C_t)\right]}{\left[4R^2L(C_{g2} + C_t)^2\right]^2} \tag{9}$$

According to (9), when $L < 2R^2(C_{g2} + C_t)$, the derivative of the damped natural frequency is negative. This indicates that the damped natural frequency is negatively correlated with the insulation capacitance C_{g2} under this condition. According to (6), to meet the above condition, the damping ratio ξ needs to be less than $\sqrt{1/2}$ (the optimal damping ratio for a second-order system). The system transfer function of the machine studied in this paper was identified based on the experimental data, as shown in (26). Consequently, the damping ratio was calculated to be approximately 0.22 according to (4), which is significantly smaller than $\sqrt{1/2}$. Therefore, when C_{g2} changes, the natural frequency and the damped natural frequency change in the same trend. This paper defines an indicator (relative change in frequency), which is expressed as (10), to determine which frequency is more sensitive to the internal GW insulation aging.

$$\delta_f = \left|\frac{f - f'}{f}\right| \times 100\% = \left|1 - \frac{f'}{f}\right| \times 100\% \tag{10}$$

where f is the frequency in a healthy state, and f' is the frequency in an insulation aging state.

When the change in the internal GW insulation capacitance C_{g2} is ΔC, the relative changes in the two frequencies are expressed as (11) and (13) respectively. When $\Delta C > 0$, $0<A<1$, $B>1$, and $0<AB<1$, so $\delta_{fn} > \delta_{fd}$. Therefore, under the same internal GW insulation aging conditions, the relative change in natural frequency f_n is greater than the relative change in damped natural frequency f_d (neutral point voltage oscillation frequency). Therefore, the natural frequency is a more sensitive and superior indicator for condition monitoring compared to the neutral point voltage oscillation frequency.

$$\delta_{fn} = \left|1 - \frac{f_n'}{f_n}\right| \times 100\% \tag{11}$$

$$A = \frac{f_n'}{f_n} = \sqrt{\frac{C_{g2} + C_t}{C_{g2} + C_t + \Delta C}} \tag{12}$$

$$\delta_{fd} = \left|1 - \frac{f_d'}{f_d}\right| = |1 - AB| \times 100\% \tag{13}$$

$$B = \frac{\sqrt{1 - \xi'^2}}{\sqrt{1 - \xi^2}} = \sqrt{1 + \frac{L\Delta C}{\left[4R^2(C_{g2} + C_t) - L\right](C_{g2} + C_t + \Delta C)}} \tag{14}$$

C. Extraction of Natural Frequency

To monitor the insulation status online, it is necessary to accurately extract the natural frequency. This paper proposes a transfer function-based frequency extraction method.

As analyzed above, the output of the system with the transfer function to be identified is the neutral point voltage. The input of the system is the machine terminal CM voltage (average value of the three-phase voltages between the terminals and the midpoint of the DC bus). After obtaining the system input and output, the nonlinear least squares method can be used to identify the system transfer function, and the natural frequency can be calculated using (4). For a single-input single-output (SISO) second-order system, its transfer function can be represented by (15). The parameters to be identified are shown in (16).

$$G(s) = \frac{Y(s)}{U(s)} = \frac{b_0 s^2 + b_1 s + b_2}{s^2 + 2\xi\omega_n s + \omega_n^2} \tag{15}$$

$$\theta = [b_0, b_1, b_2, \xi, \omega_n] \tag{16}$$

Considering the discrete nature of the sampled data, the corresponding difference equation can be expressed as (17), where $\alpha_i(\hat{\theta})$ and $\beta_i(\hat{\theta})$ are nonlinear functions of the parameters to be identified. The residual can be expressed as (18). The objective of the least squares method is to determine an estimated value $\hat{\theta}$ that minimizes the sum of squares of the residual, as expressed as (19). Numerical iterations are performed using the Gauss–Newton method, and the computation terminates when the variation of the estimated parameter $\hat{\theta}$ is smaller than the predefined threshold ε.

$$\hat{y}(k,\hat{\theta}) = -\alpha_1(\hat{\theta})y(k-1) - \alpha_2(\hat{\theta})y(k-2) + \beta_0(\hat{\theta})u(k) + \beta_1(\hat{\theta})u(k-1) + \beta_2(\hat{\theta})u(k-2) \tag{17}$$

$$e(k,\hat{\theta}) = y(k) - \hat{y}(k,\hat{\theta}) \tag{18}$$

$$J(\hat{\theta}) = \sum_{k=1}^{N} e^2(\hat{\theta}) \tag{19}$$

In practical applications, a two-stage data processing strategy is employed to enhance identification accuracy:

Step 1: *Goodness-of-Fit Filtering*: To ensure reliability, a stringent threshold is set based on the observation that the goodness of fit typically exceeds 90% under stable conditions. Consequently, any data sets yielding a fitting accuracy below 90% are discarded to exclude unreliable results caused by low signal correlation or severe interference.

Step 2: *Result Averaging*: The remaining valid natural frequency estimates are averaged to suppress random measurement noise, ensuring a stable and robust insulation indicator.

D. Identification Method for Insulation Aging Degree

To accurately assess the degree of GW insulation aging, a method is proposed to identify the variation of GW insulation capacitance. This method can be divided into two main steps as follows:

Step 1: Increasing the internal GW insulation capacitance manually. According to (7), when the GW insulation capacitance changes by ΔC, the ratio of the natural frequencies before and after the variation, k_f, can be expressed as (20). Since ΔC is known and the natural frequencies can be calculated using the method proposed in this paper before and after the change, the capacitance $C = C_{g2} + C_t$ can then be determined, as shown in (21).

$$k_f = \frac{f_n}{f_n'} = \sqrt{\frac{C_{g2} + C_t + \Delta C}{C_{g2} + C_t}} \tag{20}$$

$$C = C_{g2} + C_t = \frac{\Delta C}{\left[\left(\frac{f_n}{f_n'}\right)^2 - 1\right]} \tag{21}$$

Step 2: Since C has been determined and the natural frequencies under different conditions can also be calculated, the variation of the GW insulation capacitance can be estimated according to (22).

$$\Delta C' = \left[\left(\frac{f_n}{f_n'}\right)^2 - 1\right] C \tag{22}$$

IV. Simulation Results

To verify the effectiveness of the proposed method, corresponding simulations are carried out in MATLAB/Simulink.

A. Extraction of Natural Frequency

Fig. 9 shows the system input and output voltages (neutral point voltage) within two switching cycles under healthy state. The switching frequency is 10 kHz, the modulation index is 0.5. The estimated system transfer function is expressed as (23). By using (4) and (7), the natural frequency of the system can be calculated to be approximately 293.55 kHz, which is close to the CM impedance antiresonance frequency (291 kHz), indicating that the transfer function based natural frequency extraction method is accurate. In addition, according to (4), (7) and (8), the damped natural frequency f_d can be calculated to be approximately 286.56 kHz. And the neutral point voltage oscillation frequency can be calculated through FFT to be approximately 284.09 kHz. The above results demonstrate that the system's natural frequency is closer to the CM impedance antiresonance frequency.

$$G(s) = \frac{-0.2764s^2 + 4.985 \times 10^5 s + 3.414 \times 10^{12}}{s^2 + 8.002 \times 10^5 s + 3.402 \times 10^{12}} \tag{23}$$

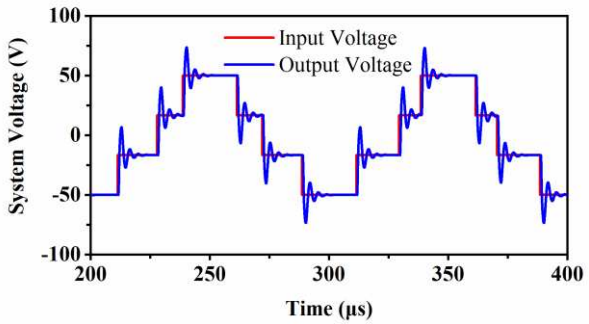

Fig. 9. Simulation results of system input and output voltage within two switching cycles under healthy state.

B. Effect of GW Insulation Aging on Natural Frequency

As in the Section III.A, GW insulation aging can be simulated by inserting a capacitor. Fig. 10 shows the neutral point voltage within one switching cycle under different degrees of internal GW insulation aging. The internal GW insulation aging affects the waveform of the neutral point voltage. Using the nonlinear least squares method, the system transfer functions for the two scenarios shown in Fig. 10 can be identified. The system transfer function in the healthy state is expressed as (23); whereas when the internal GW insulation capacitance increases by 1000 pF, the system transfer function becomes (24). By using (4) and (7), the natural frequency of the system can be calculated to be approximately 249.83 kHz for (24).

$$G(s) = \frac{-0.2591s^2 + 3.994 \times 10^5 s + 2.472 \times 10^{12}}{s^2 + 6.514 \times 10^5 s + 2.464 \times 10^{12}} \quad (24)$$

The simulation results in more scenarios are shown in Fig. 11, which show the effects of the GW insulation aging at different positions on the natural frequency, respectively. This figure further confirms that the line-end GW insulation aging has almost no effect on the natural frequency, while the internal GW insulation aging causes a variation in the natural frequency. The simulation results are consistent with the analysis in Section III.B. Therefore, by extracting the natural frequency, the internal GW insulation can be monitored.

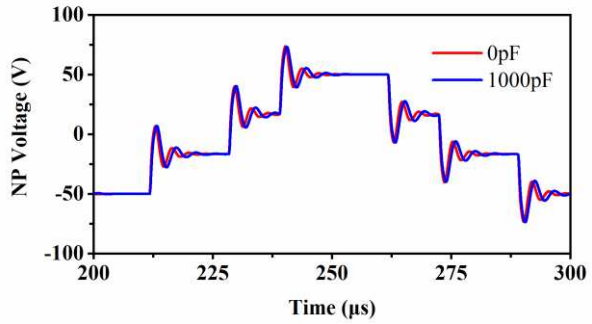

Fig. 10. Neutral point (NP) voltage within one switching cycle.

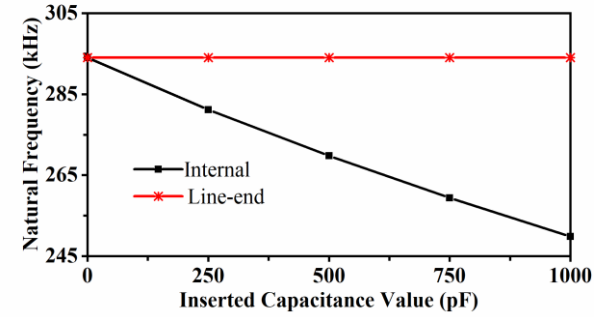

Fig. 11. Simulation results of natural frequency under GW insulation aging.

C. Identification Method for Insulation Aging Degree

Following the steps in Section III. *D*, the inserted capacitor value is 500 pF. The system's natural frequencies before and after the change are calculated, and according to (21), the capacitance C is determined to be 2716 pF. Subsequently, when the internal GW insulation capacitance value is increased by 250, 750, and 1000 pF, the estimated values of the corresponding capacitance variations can be calculated using (22). Table I presents the actual insulation capacitance variations, natural frequencies, the estimated variations, and the relative errors. The relative error is defined by (25). The simulation results demonstrate that the proposed method can reliably estimate the degree of insulation aging.

$$RE = \frac{\lfloor \Delta C - \Delta C' \rfloor}{\Delta C} \times 100\% \quad (25)$$

TABLE I
SIMULATION RESULTS OF INSULATION CAPACITANCE VARIATIONS ESTIMATION UNDER DIFFERENT AGING DEGREES

ΔC (pF)	Natural frequency (kHz)	$\Delta C'$ (pF)	Relative error (%)
250	281.12	245.49	1.80
750	259.38	762.73	1.70
1000	249.83	1033.77	3.38

V. EXPERIMENTAL RESULTS

To validate the accuracy of the proposed monitoring method, an experimental test rig is built as shown in Fig. 12. The rig primarily consists of a distributed winding PMSM from Prius 2010, a DC power supply, an Infineon SiC MOSFET-based inverter, a Plexim Rt-box 1 controller, voltage transducers with 30 MHz bandwidth. To accurately capture the HF oscillation voltage, the sampling time is 1×10^{-8} s.

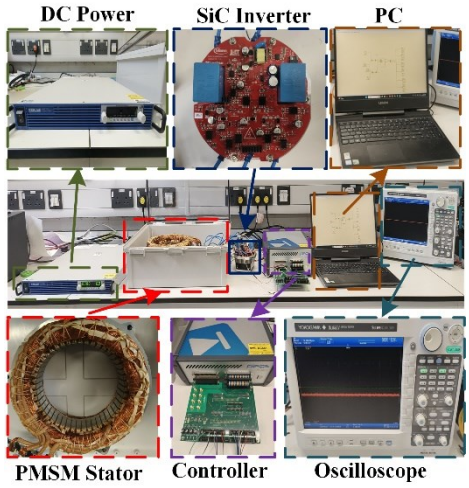

Fig. 12. Experimental test rig.

Fig. 13 shows the overall hardware platform and online GW insulation monitoring scheme. The experimental procedure is as follows. First, insulation aging is simulated by connecting a capacitor in parallel between the neutral point and the ground. Subsequently, the system output (neutral point voltage) and the system input (CM voltage at the machine input terminals) are measured respectively. To reduce the number of voltage

transducers, a resistor network can be employed, enabling the direct measurement of the system input with a single transducer. The resistor network consists of three large resistors. This configuration is commonly known as the 'virtual neutral' or 'ghost neutral', which are widely used in the field of fault diagnosis [30]. The acquired system input and output signals are then utilized to identify the system transfer function. From the identified transfer function, the system natural frequency is calculated. Finally, the status of the GW insulation is assessed based on the variations in the system natural frequency.

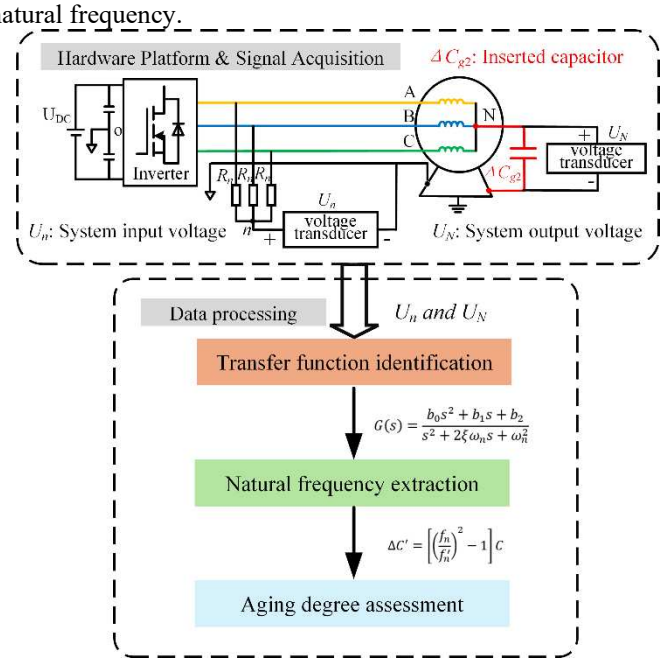

Fig. 13. Overall hardware platform and online GW insulation monitoring scheme.

A. Verification of Natural Frequency Extraction Method

Fig. 14 shows the system input and output voltages (neutral point voltage) within two switching cycles under healthy state when the switching frequency is 10 kHz. Using the nonlinear least squares method to identify the system transfer function of the input and output shown in Fig. 14, the system transfer function is expressed as (26). By using (4) and (7), the natural frequency of the system can be calculated to be approximately 292.13 kHz, which is very close to the measured CM impedance antiresonance frequency of 294 kHz. In addition, according to (4), (7) and (8), the damped natural frequency f_d can be calculated to be approximately 284.69 kHz. And the neutral point voltage oscillation frequency can be calculated through FFT to be approximately 282.95 kHz. The above results not only verify the effectiveness of the natural frequency extraction method proposed in this paper but also verify that the natural frequency is closer to the CM impedance antiresonance frequency than the neutral point voltage oscillation frequency.

$$G(s)=\frac{-0.1819s^2+6.523\times10^5 s+3.359\times10^{12}}{s^2+8.232\times10^5 s+3.369\times10^{12}} \quad (26)$$

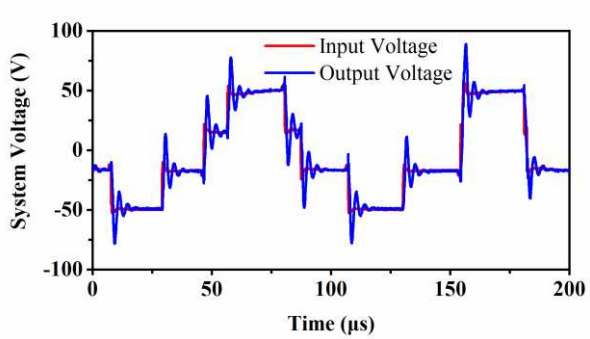

Fig. 14. Experimental results of system input and output voltage within two switching cycles under healthy state.

B. Effect of GW Insulation Aging on Natural Frequency

The GW insulation aging is simulated by connecting capacitors in parallel to ground at both the line-end and the neutral point. The inserted capacitance values are 220pF, 470 pF, 690 pF, and 940 pF. When a 470 pF capacitor is inserted at the neutral point, the system transfer function is identified using the nonlinear least squares method, and the system transfer function is expressed as (27). By using (4) and (7), the natural frequency of the system can be calculated to be approximately 271.45 kHz, which is significantly different from the natural frequency in a healthy state, 292.13 kHz.

$$G(s)=\frac{-0.1955s^2+6.039\times10^5 s+2.901\times10^{12}}{s^2+7.692\times10^5 s+2.909\times10^{12}} \quad (27)$$

To verify the effectiveness of the proposed method, more experiments have been conducted, and the results are shown in Fig. 15. It can be observed that the internal GW insulation aging causes a variation in the natural frequency, whereas the line-end GW insulation aging does not. When the capacitance increases, the natural frequency decreases, which is consistent with the analysis in Section III.

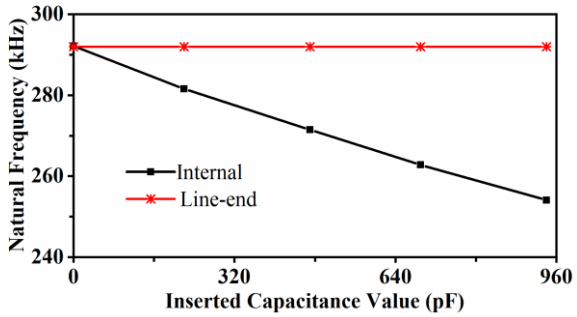

Fig. 15. Experimental results of natural frequency under GW insulation aging.

C. Verification of Identification Method for Insulation Aging Degree

Following the identification method described in Section III.*D*, a 470 pF capacitor is initially connected at the neutral point, and the corresponding natural frequency is computed. Using (21), the value of C is determined to be 2971 pF. Subsequently, when capacitors of 220, 690, and 940 pF are inserted at the neutral point, the variation in capacitance can be estimated using (22). Table II presents the actual insulation capacitance variations, natural frequencies, the estimated

variations, and the relative errors. As can be seen from the table, the relative error in the estimated variation value does not exceed 3%. The experimental results demonstrate that the proposed method can reliably estimate the degree of insulation aging.

TABLE II
EXPERIMENTAL RESULTS OF INSULATION CAPACITANCE VARIATIONS ESTIMATION UNDER DIFFERENT AGING DEGREES

ΔC (pF)	Natural frequency (kHz)	$\Delta C'$ (pF)	Relative error (%)
220	281.60	226.35	2.89
690	262.81	699.89	1.43
940	254.07	956.79	1.79

D. Comparative Analysis

Currently, most studies focus on monitoring the overall insulation of the winding or the line-end coil insulation. Reference [24] first proposed using FFT to extract the neutral point voltage oscillation frequency to monitor the internal insulation of the winding. Furthermore, it was noted in [24] that the frequency extraction accuracy of FFT is susceptible to waveform aliasing; and hence only the neutral-point voltage during zero-vector intervals was selected for FFT analysis. However, as the modulation index or switching frequency of the inverter increases, the duration of the zero-vector allocation decreases, and the aliasing issue persists, thereby compromising the extraction precision of FFT. Fig. 16 shows the waveform of the neutral point voltage at a switching frequency of 50 kHz when the insulation is healthy. Compared with the neutral point voltage at a switching frequency of 10 kHz, the waveform aliasing is obvious.

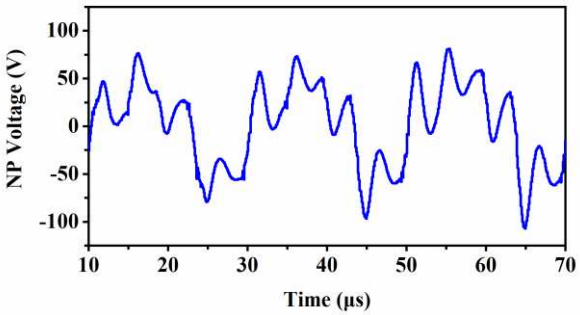

Fig. 16. Neutral point (NP) voltage at a switching frequency of 50 kHz under healthy state.

Fig. 17 illustrates the variation of the oscillation frequency extracted by FFT under healthy insulation conditions as a function of the modulation index and switching frequency. The gray plane represents the theoretical value plane. It can be observed that the frequency extraction results become inaccurate as the modulation index or switching frequency increases. Fig. 18 illustrates the natural frequency extraction results obtained by the proposed transfer-function-based method. It can be observed that the proposed method in this paper is minimally affected by the modulation index and switching frequency.

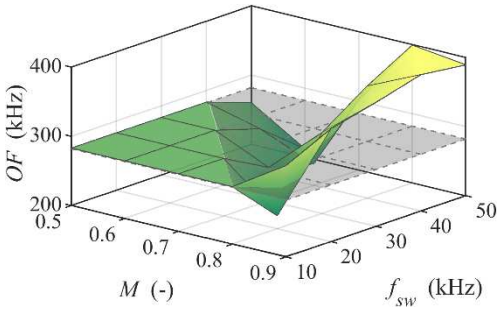

Fig. 17. Oscillation frequency (*OF*) extracted by FFT under healthy insulation condition versus modulation index (*M*) and switching frequency (f_{sw}).

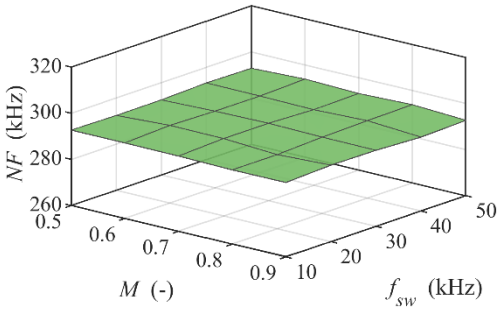

Fig. 18. Natural frequency (*NF*) under healthy insulation condition versus modulation index (*M*) and switching frequency (f_{sw}).

For a better comparison, Table III presents the actual insulation capacitance variation, estimated change, and relative error for both methods, under the condition of a 0.8 modulation index and a 40 kHz switching frequency. Specifically, negative values indicate a decrease in the estimated insulation capacitance. As demonstrated in Table III, when waveform aliasing occurs due to the increase in switching frequency and modulation index, the conventional FFT-based method in [24] becomes ineffective. In contrast, the method proposed in this paper maintains high identification accuracy. Therefore, the method proposed in this paper has strong robustness.

TABLE III
COMPARISON OF CAPACITANCE VARIATION ESTIMATION FOR THE TWO METHODS AT M=0.8 AND F_{SW}=40 KHZ

ΔC (pF)	$\Delta C'$ (pF) [24]	Relative error (%)	$\Delta C'$ (pF) [Proposed]	Relative error (%)
220	-902.11	510	228.83	4.01
690	-1580.15	329	709.60	2.84
940	-1099.82	217	958.99	2.02

E. Case Study Using a Concentrated Winding PMSM

To verify the applicability of the proposed method, experiments were also conducted on a concentrated winding PMSM from [31]. The extraction results of natural frequency under different aging degrees are shown in Fig. 19. When the GW insulation is in a healthy state, the natural frequency is 277.87 kHz. Following the identification method described in Section III.D, a 470 pF capacitor is initially connected at the neutral point, and the corresponding natural frequency

changes to 220.02 kHz. Using (21), the value of C is determined to be 790 pF. Subsequently, when capacitors of 220, 330, and 690 pF are inserted at the neutral point, the variation in capacitance can be estimated using (22). Table IV presents the actual insulation capacitance variations, natural frequencies, the estimated variations, and the relative errors, under the condition of a 0.5 modulation index and a 10kHz switching frequency. Experimental results show that the method proposed in this paper is also suitable for a concentrated winding machine.

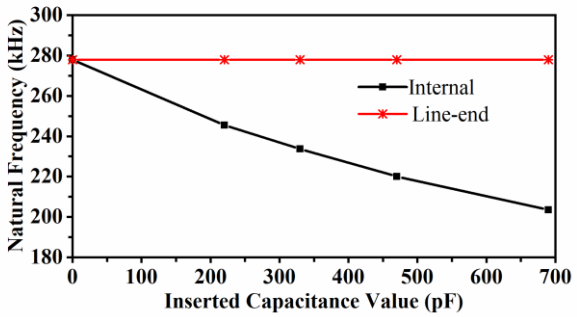

Fig. 19. Natural frequency with a concentrated winding PMSM from [31].

TABLE IV
CAPACITANCE VARIATIONS ESTIMATION WITH A CONCENTRATED WINDING PMSM FROM [31].

ΔC (pF)	Natural frequency (kHz)	$\Delta C'$ (pF)	Relative error (%)
220	245.41	222.81	1.28
330	233.66	327.23	0.84
690	203.57	681.92	1.17

VI. CONCLUSION

Extensive research has been conducted over the years on the line-end GW insulation degradation caused by line-end overvoltage. However, recent studies have revealed that significant overvoltage also exists inside the windings, which can likewise deteriorate the internal GW insulation. To address this issue, this paper proposes a corresponding monitoring method. Firstly, the influence of GW insulation aging at different positions on the CM spectrum has been studied based on the winding HF model established in this paper. Then, the relationship between the natural frequency of the CM circuit and the antiresonance frequency of CM impedance has been revealed. Based on this relationship, an internal GW insulation monitoring method based on the natural frequency has been proposed. Besides, to accurately extract the natural frequency, a transfer function-based frequency extraction method has been proposed. This method considers the neutral point voltage as the output of a second-order system to be identified, while the input is the average of the three-phase input voltages. The nonlinear least squares method can be used to identify the system transfer function, and the denominator of the second-order system transfer function can be used to calculate the natural frequency. In addition, the effects of modulation index and switching frequency on the proposed method and existing method have been investigated.

It is found that the internal GW insulation aging changes the antiresonance frequency of CM spectrum, while the line-end GW insulation aging does not. Besides, this paper has shown that natural frequency of the second-order system formed by the windings is equal to the CM antiresonance frequency. Since the natural frequency is easier to obtain than the CM impedance antiresonance frequency, the GW insulation monitoring method based on the natural frequency is proposed. This method can quantitatively monitor the internal GW insulation aging without being affected by the line-end GW insulation aging. The proposed frequency extraction method has strong robustness and is not affected by switching frequency and modulation index, which is superior to existing methods. The effectiveness of the proposed frequency extraction and internal GW insulation monitoring methods is validated through both simulation and experiments on PMSMs with distributed and concentrated windings.

The main limitation of the proposed method in this paper is that it depends on the ability to physically access the machine's neutral point for the acquisition of the output voltage. The method is not immediately applicable to delta-connected windings or internal star-connected systems lacking a neutral point access terminal. Future research will focus on addressing this limitation.

APPENDIX

Stator outer diameter = 264 mm, stator inner diameter = 161.9 mm, stack length = 50.8 mm, slot depth = 30.9 mm, slot opening = 1.88 mm, number of slots = 48, series coils of one phase = 8, turns of one coil = 11, number of wires in parallel of one turn = 12, wire size = 20 AWG, thickness of turn insulation = 0.025 mm, relative permittivity of turn insulation = 3.5, relative permittivity of GW insulation = 3.5.

REFERENCES

[1] Z. Xu, J. Zhang, J. Xiong, Y. Wu and M. Cheng, "An Improved High-Frequency Voltage Injection Method for Interturn Short-Circuit Fault Detection in PMSMs," *IEEE Trans. Transport. Electrific*., vol. 9, no. 2, pp. 3228-3239, Jun 2023.
[2] R. Tao, W. Wang, Y. Jiang, C, Tang, Y. Fan, and W. Hua, "Free-Current-Curve Fault-Tolerant Control of Dual Three-Phase Permanent Magnet Synchronous Motor Under Open-Phase Fault," *IEEE Trans. Transport. Electrific*., vol. 11, no. 5, pp. 11619-11631, Oct. 2025.
[3] X. Xu, J. Hang, K. Cao, S. Ding and W. Wang, "Unified Open-Phase Fault Diagnosis of Five-Phase PMSM System in Normal Operation and Fault-Tolerant Operation Modes," *IEEE Trans. Transport. Electrific*., vol. 11, no. 5, pp. 12063-12075, Oct. 2025.
[4] S. Sundeep, J. Wang, and A. Griffo, "Holistic Modeling of High-frequency Behavior of Inverter-fed Machine Winding, Considering Mutual Couplings in Time Domain," *IEEE Trans. Ind. Appl*., vol. 57, no. 6, pp. 6044-6057, Nov/Dec. 2021.
[5] G. Stone, "Condition Monitoring and Diagnostics of Motor and Stator Windings–A Review," *IEEE Trans. Dielectr. Electr. Insul*., vol. 20, no. 6, pp. 2073-2080, Dec. 2013.
[6] A. Gandhi, T. Corrigan, and L. Parsa, "Recent Advances in Modeling and Online Detection of Stator Interturn Faults in Electrical Motors," *IEEE Trans. Ind Electron*., vol. 58, no. 5, pp. 1564-1575, May. 2010.

[7] M. Sumislawska, K. N. Gyftakis, D. F. Kavanagh, M. D. McCulloch, K. J. Burnham, and D. A. Howey, "The Impact of Thermal Degradation on Properties of Electrical Machine Winding Insulation Material," *IEEE Trans. Ind. Appl*., vol. 52, no. 4, pp. 2951-2960, Jul/Aug. 2016.

[8] S. B. Lee, K. Younsi, and G. B. Kliman, "An online technique for monitoring the insulation condition of AC machine stator windings," *IEEE Trans. Energy Convers*., vol. 20, no. 4, pp. 737-745, Dec. 2005.

[9] Gonzalez, J. M., Rodrigues, L. K., Beza-Florentin, F., Butnaru, C., Mikula, M., Neves, A., and Sarrico, J. V. "A Methodology for Accelerated Thermal Aging of an Automotive Hairpin Stator", *IEEE Trans. Dielectr. Electr. Insul.,* vol. 32, no. 4, Aug. 2025.

[10] P. Zhang, K. Younsi, and P. Neti, "A Novel Online Stator Ground-wall Insulation Monitoring Scheme for Inverter-fed AC Motors," *IEEE Trans. Ind. Appl*., vol. 51, no. 3, pp. 2201-2207, May/Jun. 2015.

[11] D. Zheng, and P. Zhang, "An Online Groundwall and Phase-to-phase Stator Insulation Monitoring Method for Inverter-fed Machine," *IEEE Trans. Ind. Electron*., vol. 68, no. 6, pp. 5303-5313, Jun. 2021.

[12] P. Zhang, D. Zheng, and G. Lu, "The Effect and Compensation of Phase Angle Deviation Along the Winding for the Online Stator Insulation Condition Monitoring," *IEEE Trans. Ind. Electron.*, vol. 69, no. 8, pp. 8440-8451, Aug. 2022.

[13] G. C. Stone, "A Perspective on Online Partial Discharge Monitoring for Assessment of the Condition of Rotating Machine Stator Winding Insulation," *IEEE Elect. Insul Mag*., vol. 28, no. 5, pp. 8-13, Sep/Oct. 2012.

[14] D. Zheng, G. Lu, and P. Zhang, "An Improved Online Stator Insulation Monitoring Method Based on Common-mode Impedance Spectrum Considering the Effect of Aging Position," *IEEE Trans. Ind. Appl*., vol. 58, no. 3, pp. 3558-3566, May/Jun. 2022.

[15] P. Neti, and S. Grubic, "Online Broadband Insulation Spectroscopy of Induction Machines Using Signal Injection," *IEEE Trans. Ind. Appl*., vol. 53, no. 2, pp. 1054-1062, Mar/Apr. 2016.

[16] F. Niu, Y. Wang, S. Huang, L. Wu, X. Huang, Y. Fang, and T. Yang, "An Online Groundwall Insulation Monitoring Method Based on Transient Characteristics of Leakage Current for Inverter-fed Motors," *IEEE Trans. Power Electron*., vol. 37, no. 8, pp. 9745-9753, Aug. 2022.

[17] W. R. Jensen, E. G. Strangas, and S. N. Foster, "A Method for Online Stator Insulation Prognosis for Inverter-driven Machines," *IEEE Trans. Ind. Appl.*, vol. 54, no. 6, pp. 5897-5906, Nov/Dec. 2018.

[18] C. Zoeller, M. A. Vogelsberger, R. Fasching, W. Grubelnik, and T. M. Wolbank, "Evaluation and Current-response-based Identification of Insulation Degradation for High Utilized Electrical Machines in Railway Application," *IEEE Trans. Ind. Appl*., vol. 53, no. 3, pp. 2679-2689, May/Jun. 2017.

[19] P. Nussbaumer, M. A. Vogelsberger, and T. M. Wolbank, "Induction machine insulation health state monitoring based on online switching transient exploitation," *IEEE Trans. Ind. Electron*., vol. 62, no. 3, pp. 1835-1845, Mar. 2015.

[20] D. Xiang, H. Li, H. Yan, Y. Zheng, N. Zhao, and B. Liu, "Online Monitoring of Incipient Turn Insulation Degradation for Inverter-fed Machine Using Sensitive Tail Component in PWM Switching Oscillations," *IEEE Trans. Power Electron*., vol. 36, no. 8, pp. 8730-8742, Aug. 2021.

[21] H. Li, Y. Li, D. Xiang, and Y. Li, "Online Condition Monitoring of Line-end Coil Insulation for Inverter-fed Machine by Switching Oscillation Mode Decomposition," *IEEE Trans. Ind. Electron*., vol. 69, no. 11, pp. 11697-11708, Nov. 2022

[22] H. Li, H. Yang, D. Xiang, and J. Chen, "Ultra-Sensitive Monitoring of Line-End Coil Insulation Degradation in Inverter-Fed Machine Using PT Symmetry," *IEEE Trans. Ind. Electron*., Aug. 2025.

[23] S. Sundeep, J. Wang, A. Griffo, and F. Alvarez-Gonzalez, "Antiresonance Phenomenon and Peak Voltage Stress Within PWM Inverter Fed Stator Winding," *IEEE Trans. Ind. Electron*., vol. 68, no. 12, pp. 11826-11836, Dec. 2021.

[24] H. Li, Y. Gu, D. Xiang, P. Zhang, P. Yue, and Y. Cui, "Online Condition Monitoring of Winding Internal Insulation for Inverter-fed Machine Using Neutral-to-ground High-frequency Switching Oscillation Voltage," *Proc. CSEE*, vol. 44, no. 2, pp. 817–826, Jan. 2024.

[25] B. Mirafzal, G. L. Skibinski, and R. M. Tallam, "Determination of Parameters in the Universal Induction Motor Model," *IEEE Trans. Ind. Appl*., vol. 45, no. 1, pp. 142-151, Jan/Feb. 2009.

[26] Y. Xie, J. Zhang, F. Leonardi, A. R. Munoz, M. W. Degner, and F. Liang, "Voltage Stress Modeling and Measurement for Random-wound Machine Windings Driven by Inverters," *IEEE Trans. Ind. Appl*., vol. 56, no. 4, pp. 3536-3548, Jul. 2020.

[27] D. A. Hewitt, S. Sundeep, J. Wang, and A. Griffo, "High Frequency Modeling of Electric Machines Using Finite Element Analysis Derived Data," *IEEE Trans. Ind. Electron*., vol. 71, no. 2, pp. 1432-1442, Feb. 2023.

[28] C. R Paul, Analysis of Multiconductor Transmission Lines, John Wiley& Sons Inc., 2nd Edition, New Jersey, USA, 2007.

[29] H. Li, J. Chen, D. Xiang and R. Cheng, "Offline quantitative evaluation of electrical machine insulation through common-mode impedance resonance frequency perturbation", *IEEE Trans. Ind. Electron.*, vol 71, no. 8, pp. 9687-9697, Aug. 2024.

[30] J. Hang, J. Zhang, M. Cheng, and J. Huang, "Online Interturn Fault Diagnosis of Permanent Magnet Synchronous Machine Using Zero-Sequence Components," *IEEE Trans. Power Electron*., vol. 30, no. 12, pp. 6731-6741, Dec. 2015.

[31] W. Zhu, D. Gaetano, X. Sun, H. Li, X. Chen and A. Griffo, "Localized Asymmetric Behavior of Common-Mode Current Through Bearing Balls", *IEEE Trans. Energy Convers*, 2025.